HHS Public Access

Author manuscript

Cell Stem Cell. Author manuscript; available in PMC 2016 August 24.

Published in final edited form as:

Cell Stem Cell. 2016 July 7; 19(1): 95–106. doi:10.1016/j.stem.2016.05.002.

Functional coupling with cardiac muscle promotes maturation of hPSC-derived sympathetic neurons

Yohan Oh[1,2,3], **Gun-Sik Cho**[1,4], **Zhe Li**[5], **Ingie Hong**[5], **Renjun Zhu**[6], **Min-Jeong Kim**[1,2,9], **Yong Jun Kim**[1,2,10], **Emmanouil Tampakakis**[4], **Leslie Tung**[6], **Richard Huganir**[5], **Xinzhong Dong**[5,7,8], **Chulan Kwon**[1,4,*], and **Gabsang Lee**[1,2,3,4,*]

[1]Institute for Cell Engineering, Johns Hopkins University School of Medicine, Baltimore, MD 21205, USA

[2]Department of Neurology, Johns Hopkins University School of Medicine, Baltimore, MD 21205, USA

[3]Adrienne Helis Malvin Medical Research Foundation, New Orleans, LA 70130, USA

[4]Division of Cardiology, Johns Hopkins University School of Medicine, Baltimore, MD 21205, USA

[5]The Solomon H. Snyder Department of Neuroscience, Johns Hopkins University School of Medicine, Baltimore, MD 21205, USA

[6]Department of Biomedical Engineering, The Johns Hopkins University, Baltimore, MD 21205, USA

[7]Center for Sensory Biology, Johns Hopkins University School of Medicine, Baltimore, MD 21205, USA

[8]The Howard Hughes Medical Institute, Baltimore, MD 21205, USA

Summary

Neurons derived from human pluripotent stem cells (hPSCs) are powerful tools for studying human neural development and diseases. Robust functional coupling of hPSC-derived neurons with target tissues in vitro is essential for modeling intercellular physiology in a dish and to further translational studies, but has proven difficult to achieve. Here, we derive sympathetic neurons from hPSCs and show they can form physical and functional connections with cardiac muscle cells. Using multiple hPSC reporter lines, we recapitulated human autonomic neuron development in vitro and successfully isolated PHOX2B:eGFP+ neurons that exhibit sympathetic marker expression and electrophysiological properties, and norepinephrine secretion. Upon pharmacologic

[*]Correspondence: glee48@jhmi.edu and ckwon13@jhmi.edu.

[9]Present Address: Stem Cell & Regenerative Medicine Institute, Research Institute for Future Medicine, Samsung Medical Center, Seoul 06351, Korea

[10]Present Address: Department of Pathology, College of Medicine, Kyung Hee University, Seoul, 130-701, Korea

Contact Information

Dr. Gabsang Lee, glee48@jhmi.edu, Phone: +1-443-287-8631, Fax: +1-410-614-9568

Author Contributions

Conceptualization, Y.O., C.K., and G.L.; Methodology, Y.O., G.-S.C., Z.L., I.H., R.Z., M.-J.K., Y.J.K., E.T., L.T., R.H., X.D., C.K., and G.L.; Formal Analysis, Y.O., Z.L., I.H., and R.Z.; Investigation, Y.O., G.-S.C., Z.L., I.H., R.Z., M.-J.K., Y.J.K., and E.T.; Resources, Y.O., G.-S.C., Z.L., I.H., R.Z., M.-J.K., Y.J.K., and E.T.; Writing - Original Draft, Y.O. and G.L.; Writing - Review & Editing, Y.O., C.K., and G.L.; Visualization, Y.O.; Supervision, C.K. and G.L.; Funding Acquisition, C.K. and G.L.

and optogenetic manipulation, PHOX:eGFP+ neurons controlled beating rates of cardiomyocytes, and the physical interactions between these cells increased neuronal maturation. This study provides a foundation for human sympathetic neuron specification and for hPSC-based neuronal control of organs in a dish.

Introduction

Sympathetic neurons originate from neural crest cells and control the functions of vital organs as part of the autonomic nervous system (ANS) (Anderson et al., 1997; Bhatt et al., 2013). When the sympathoadrenal neural crest cells migrate along the ventromedial path, they are exposed to the morphogens sonic hedgehog proteins (SHH) and bone morphogenetic proteins (BMP) sequentially, which are secreted from the notochord and aorta region respectively (Anderson et al., 1997; Bhatt et al., 2013). The migrated neural crest cells initially form a continuous sympathetic chain. This chain segregates into discrete ganglia and differentiates into sympathetic neurons that innervate various targets, including cardiac tissues, blood vessels, glands and smooth muscle (Bhatt et al., 2013; Takahashi et al., 2013). Aberrant activity and dysfunction of the sympathetic neurons contribute to the pathophysiology of human hypertension and cardiac conditions (Kimura et al., 2012), diabetes mellitus (Vinik et al., 2003), Parkinson's disease (Chaudhuri, 2001), and familial dysautonomia (Axelrod et al., 2002; Rotthier et al., 2012).

Although animal models are widely used to study human autonomic neurons and related disorders, they have significant limitations due to the inter-individual genetic heterogeneity and distinct homeostatic mechanisms between rodents and humans. Neurons derived from human pluripotent stem cells (hPSCs), including embryonic stem or induced pluripotent stem cells (hESCs/hiPSCs), have emerged as a promising model for studying human neural development and disease (Brennand et al., 2011; Dimos et al., 2008; Laflamme et al., 2007; Li et al., 2005; Maroof et al., 2010), and could be used as cell sources for transplantation (Cunningham et al., 2014; Joseph and Morrison, 2005). While significant and rapid progress has been made on the generation and utilization of central nervous system cell types differentiated from hPSCs (Li et al., 2005; Perrier et al., 2004), very few studies have been reported on peripheral neural derivation (Lee et al., 2007; Schrenk-Siemens et al., 2015). Moreover, it remains unknown whether a defined population of peripheral neurons can be isolated from hPSCs. Although a recently report presented the generation of functional neuromuscular junction using hPSCs-derived spinal motor neurons and skeletal muscle fibers (Steinbeck et al., 2016), it remains unknown whether hPSC-derived peripheral neurons can mimic neuromodulatory function with their target tissues.

Creating a reporter 'knock-in' system in hPSCs is a powerful approach for monitoring hPSC differentiation toward specific cell types, and for isolating the resulting cells. The CRISPR/Cas9 system (Cong et al., 2013; Mali et al., 2013), offers targeted genome editing and can be used to efficiently generate hPSC lines harboring gene reporters. This can be applied for monitoring the development of a specific subtype of neurons, which would be beneficial for the studies of human sympathetic neuronal development and related human diseases.

Here, we recapitulated the sympathoadrenal differentiation process *in vitro* by developing multiple genetic reporters and demonstrated the successful differentiation and isolation of sympathetic progenitors and neurons from hPSCs. The sympathetic neuron identity was confirmed by gene expression analysis and physiological and functional activity. Furthermore, the resulting neurons showed physical and functional connectivity with heart muscle cells, leading to neuronal maturation.

Results

WNT and SHH Signaling Enhance Both Expression Levels of ASCL1 and PHOX2B in hPSC-Derived Autonomic Specification

The basic helix-loop-helix (bHLH) transcription factor ASCL1 and homeodomain transcription factor PHOX2B are key transcription factors essential for sympathetic neuronal development (Hirsch et al., 1998; Pattyn et al., 2000). To test whether sympathetic neurons can be induced from hPSCs, we established two genetic reporter lines expressing green fluorescent protein (GFP) from the loci of *ASCL1* and *PHOX2B*, *i.e.*, *ASCL1::eGFP* and *PHOX2B::eGFP* hESCs (Figure 1A–1F). The gene targeting strategy was to replace each stop codon of the *ASCL1* and *PHOX2B* genes with 2A-eGFP-PGK-Puro^R gene cassettes through homologous recombination enhanced by the CRISPR/Cas9 system (Cong et al., 2013; Mali et al., 2013) (Figure 1A and 1D). After selecting phenotypically and karyotypically normal lines (Figure 1B, 1E, and S1A–S1B), we searched for sympathetic neuronal differentiation. In animal models, specification of sympathetic neurons and chromaffin cells are specified from migrating neural crest stem cells by SHH and BMP signaling (Morikawa et al., 2009; Schneider et al., 1999). We initially induced neural crest cells using SMAD inhibition (termed ‘LSB’ for inhibitors LDN193189 and SB431542) protocol (Chambers et al., 2009). Similar to the *in vivo* process, expression levels of ASCL1::eGFP and PHOX2B::eGFP were significantly enhanced with recombinant sonic hedgehog C25II (Shh) protein and SHH agonist (purmorphamine, PMP), and significantly decreased by treatment with an SHH antagonist (cyclopamine, CyP) (Figure 1G and S1C–S1D). In addition, BMP4 treatment from day 10 significantly increased the expression of ASCL1 and PHOX2B (Figure 1H). Mica *et al.* showed that WNT activation using CHIR99021 combined with the LSB method augments the proportion of neural crest cells in the population (Mica et al., 2013). Similarly, we also found that transient WNT activation (started a day before the activation of SHH signaling) induces both ASCL1::eGFP and PHOX2B::eGFP expression (Figure 1I). To accelerate neural crest specification and peripheral neuron formation from neural crest cells, we adopted the combined three small molecules protocol (CHIR99021, DAPT, and SU5402, called 3i for ‘three inhibitors’) (Chambers et al., 2012) and modified it with substitution of PD173074 for SU5402 (modified-3i or m3i). We observed significantly higher levels of ASCL1::eGFP and PHOX2B::eGFP expression with the m3i treatment than with the CHIR99021 single treatment (Figure 1I). The numbers of ASCL1::eGFP and PHOX2B::eGFP cells were also greatly increased with m3i treatment followed by BMP4 (46.43 ± 0.54% and 4.13 ± 0.18%, respectively) (Figure 1J). The eGFP expression of both reporter lines was detectable either by the FACS analysis, immunocytochemistry, or live cell imaging, and mostly co-localized with endogenous ASCL1 or PHOX2B proteins (Figure 1C, 1F, 1K, and S1E–S1G). Some

PHOX2B-expressing cells began to show neurite outgrowth from day 10 after differentiation (Figure 1K, right panels; S1G). Post-sorting qRT-PCR showed the enrichment of transcripts expressed in sympathetic neuron and/or chromaffin cells specification, indicating a proper lineage specification (Figure 1L). We further generated a *PHOX2B::eGFP* reporter hiPSC line and produced PHOX2B::eGFP+ cells from hiPSCs using the same neuronal specification protocol (Figure S1H). Together, these results showed that the activation of WNT followed by SHH signaling leads to the generation of both *ASCL1*- and *PHOX2B*-expressing sympathetic progenitors and neurons from hPSCs.

Global Gene Expression Changes during Sympathetic Neuronal Differentiation

The dynamics of global gene expression during sympathoadrenal differentiation remains largely unknown even in animal models. Using the four genetic reporter systems (*OCT4::eGFP* (Figure S1I), *SOX10::eGFP* (Figure S1J), *ASCL1::eGFP*, and *PHOX2B::eGFP* reporter hESC lines), we were able to purify discrete cell populations at four differentiation stages, recapitulating the sympathoadrenal differentiation process *in vitro* with purified and defined populations in four specific differentiation stages (Figure 2A). We performed transcriptome analysis of OCT4::eGFP+ cells (representing undifferentiated hESCs), SOX10::eGFP+ cells (multi-potent neural crest), ASCL1::eGFP+ cells (putative sympathoadrenal progenitors), and PHOX2B::eGFP+ cells (putative sympathetic neuronal precursors) shown by the hierarchically clustering heat map (Figure 2B). Each of the four purified populations had unique gene expression patterns associated with their cellular identities (Figure 2C–2F and S2A–S2D). Other groups have reported that *ASCL1* and *PHOX2B* are genetically correlated with each other during murine ANS development (Hirsch et al., 1998; Huber et al., 2002; Pattyn et al., 2000). Consistently, our data also demonstrated that ASCL1::eGFP+ and PHOX2B::eGFP+ cells share similar patterns of gene expression (Figure 2B and 2E). However, gene ontology (GO) analysis and differential gene expression data indicated that ASCL1::eGFP+ cells are specified earlier than PHOX2B::eGFP+ cells during sympathetic neuronal development (Figure 2F–2H, S2C–S2D, and S2G). Additionally, we verified sets of transcriptomes that are associated with the specification of sympathoadrenal lineage cells (Figure 2E and S2A–S2C), and identified signature genes involved in the sympathetic neuronal specification (Figure 2F and S2D), and gene sets of two relevant diseases (dysautonomia and neuroblastoma) (Figure S2E–S2F). ASCL1::eGFP+ and PHOX2B::eGFP+ cells expressed higher levels of PNMT and chromogranin A (CHGA) (Figure 1L and 2E), suggesting the presence of sympathoadrenal progenitors (Huber, 2015). Indeed, these cells could give rise not only to sympathetic neuronal cells, but also to ‘chromaffin-like’ cells (Figure S2H). Together, these data show the feasibility of modeling human sympathetic development with hPSCs.

Characterization of PHOX2B::eGFP+ Neurons from hPSCs

With this established protocol, we successfully guided hPSCs to become putative sympathetic neurons (Figure 3). Sorted PHOX2B::eGFP+ cells were further differentiated into PHOX2B, peripherin (PRPH), TH, DBH, GATA3, ISL1, and nicotinic acetylcholine receptors (nAChRs)-expressing putative sympathetic neurons (Figure 3A–3C and S3A–S3D). These cells expressed sympathetic neuronal genes after differentiation (Figure 3D) and showed negligible percentages of HB9-expressing motor neurons (0.54 ± 0.42% of

cells) and BRN3A-expressing sensory neurons (0.89 ± 0.28% of cells) (Figure S3E–S3F and S3J). Based on this information, we were able to obtain sympathetic neurons without cell sorting. Differentiated parental hPSCs (genetically unmodified) could give rise to cells expressing ASCL1 and PHOX2B (Figure S3K), and subsequently yield TH/DBH/GATA3/PRPH-expressing and catecholamines-releasing neurons from hPSCs (Figure S3M–S3P) with a similar protocol as described (Figure S3L). In addition, FACS-purified ASCL1::eGFP + cells were maintained over 150 days and differentiated into ASCL1/TH/DBH/GATA3/PRPH-expressing neurons (Figure S3Q–S3V). To test whether the neurons differentiated from sorted PHOX2B::eGFP+ cells were electrophysiologically functional, we subsequently performed a whole-cell patch-clamp analysis. As shown in Figure 3E, these neurons expressed a considerable amount of Na^+ channels and K^+ channels for conducting both inward and outward currents. These neurons were able to fire an action potential (AP) train when 50 mM KCl was added to the bath (Figure 3F), and the hESC-derived putative sympathetic neurons also responded to nicotine, which directly binds and activates nAChRs of post-ganglionic sympathetic neurons (Figure S3G–S3H). Upon current injecting, the neurons fired a single AP (Figure 3G, left panel; Type 1, ‘phasic’) or a train of APs (Figure 3G, right panel; Type 2, ‘tonic’), and exhibited a medium afterhyperpolarization (AHP) (Figure 3H) with the amplitude and duration of which were 12.1 ± 1.2 mV and 291.1 ± 55.8 ms respectively ($n = 3$) and the resting membrane potential (RMP) of −46.2 ± 5.4 mV ($n = 12$) in sorted PHOX2B::eGFP+ cells. We tested whether the depolarization of these neurons was dependent on Ca^{2+} and/or Na^+ ions. As expected, the AP of these neurons was partially blocked with Cd^{2+} (non-specific Ca^{2+} channel blocker) alone, and completely blocked with Cd^{2+} + TTX (voltage-dependent Na^+ channel blocker), showing the dependence on both Ca^{2+} and Na^+ ions (Figure S3I). These data suggest hPSC-derived sympathetic neurons possess electrophysiological properties similar to rodent sympathetic neurons (Anderson et al., 2001; Jobling and Gibbins, 1999). Finally, we found that the PHOX2B::eGFP+ neurons released significantly higher levels of dopamine (DA) and norepinephrine (NE), of which levels were significantly higher than in hESC-derived PRPH/ISL1/BRN3A/RUNX1-expressing sensory neurons (Figure 3I and S3J). Taken together, these results demonstrate the feasibility of directing hPSCs into functional NE-secreting sympathetic neurons *in vitro*.

Pharmacological Neural Control of Cardiac Ventricular Myocytes

To examine neuronal functionality and to test sympathetic connections *in vitro*, we co-cultured FACS-purified PHOX2B::eGFP+ sympathetic neurons with neonatal mouse ventricular myocytes (NMVM), mESC- or hiPSC-derived cardiomyocytes (Figure 4A and S4A–S4I). Through morphological, ultrastructural, and immunofluorescence analyses, we found that the neurons form direct physical contact with cardiomyocytes (Figure 4B–4C, S4A–S4I; Movie S1). In particular, as shown in transmission electron microscopy (Figure 4B), hPSC-derived PHOX2B::eGFP+ neurons started to form synaptic connections with a few putative synaptic vesicles, although their synaptic structure appeared to be underdeveloped. To address whether these connections can be made with other cell type, we have performed co-cultured the neurons and C2C12 skeletal myotubes as a negative control (Figure S4J–S4K). We only detected one SV2 positive myotube out of 412 myotubes, suggesting that the hPSC-derived sympathetic neurons may have target specificity. We found that nicotine treatment (1 μM, stimulating sympathetic neurons only) affected the beating

rate of NMVM in the presence of the hESC-derived sympathetic neurons (Figure 4D, *iii*; 4E–4F). However, the effect was not observed any of the four control groups: NMVM only (Figure 4D, *i*), sensory neurons with NMVM (Figure 4D, *ii*), co-cultured on separate coverslips (Figure 4D, *iv*), or NMVM cultured with the conditioned medium of activated sympathetic neurons (Figure S4N), indicating that the direct connections between neurons and NMVM are important to affect the beating rate of NMVM. In addition to chronotropic effect of nicotine, inotropic effect was also detected on this co-culture system (Figure S4L). Moreover, we found that nicotine treatment in co-culture caused a slight but significant AP shortening (Figure S4M). In contrast, the propagation of APs and beating synchronization were not altered after neuronal stimulation by nicotine (Movie S2 and S3).

Optogenetic Neural Control of Cardiac Ventricular Myocytes

To test whether their neuronal activity can be controlled by optogenetic stimulations, we transduced PHOX2B::eGFP+ neurons with lentiviral vectors expressing hChR2-eYFP (Figure 5A–5F and S5A–S5B). hChR2-eYFP expression in TH-positive putative sympathetic neurons were confirmed by immunostaining (Figure 5B–5D). In addition, hChR2-expressing neurons fired light-induced APs over a broad frequency range from 1 to 10 Hz (Figure 5E and S5B). Spike fidelity was increased with increasing light intensity (Figure S5A). Furthermore, photostimulation in the hChR2-expressing PHOX2B::eGFP+ sympathetic neurons led to NE secretion (Figure 5F). Next, we test whether spontaneous beating rates of co-cultured NMVM with human sympathetic neurons, can be controlled optogenetically. The beating rate of NMVM could be optogenetically controlled with hChR2-expressing hESC-derived sympathetic neurons when they were in physical contact with cardiomyocytes (Figure 5G, *iii*; Movie S4). Following optogenetic activation of neurons, the beating rates of NMVM were quickly dialed up, while immediately down after stimulation (Figure 5I and Movie S4). In contrast, there was no response to light exposure in any of the three control groups: NMVM only (Figure 5G, *i*), eGFP-expressing neuron with NMVM (Figure 5G, *ii*), or stimulating non-connected neuron with NMVM (Figure 5G, *iv*). However, the optogenetic stimulation-induced beating rate increment of NMVM was significantly blocked by the β-blocker, propranolol (Figure 5H and S5C). These data demonstrate that PHOX2B::eGFP+ neurons form physical and functional connections with ventricular myocytes, and these β-adrenergic connections allow pharmacological and optogenetic control of the PHOX2B::eGFP+ neurons to influence cardiac contractile behaviors.

Physical Interaction Leads to Neuronal Maturation Phenotypes

Functional connections between neurons and their target tissues are known to promote neuronal maturation during development (Bharmal et al., 2001; Devay et al., 1999). To test these, we analyzed the ability of the PHOX2B::eGFP+ neurons to release neurotransmitters when co-cultured with or without NMVM. The co-cultured neurons released significantly more NE, and expressed significantly higher levels of enzymes crucial for catecholamine synthesis than did neurons cultured without NMVM (Figure 6A–6B and S6A). In addition, the expression of nAChRs and sodium and potassium channels were significantly increased in the co-cultured neurons with NMVM compared to those cultured alone (Figure 6C and S6D), which is consistent with the enhanced sensitivity to nicotine (0.1 μM) (Figure 6D–6G

and Movie S5). Furthermore, the expression levels of catecholamine-synthesizing enzymes and nAChRs were significantly higher in the co-cultured neurons with NMVM than in control neurons cultured under NMVM-conditioned medium (Figure 6B–6C). This indicates that the physical contact between the sympathetic neurons and NMVM promotes neuronal maturation. This phenotype was not observed in hPSC-derived sensory neurons co-cultured with NMVM (Figure S6B–S6C). The profiling of mouse sympathetic neurons at different developmental stages showed that expression of these genes is indeed increased during sympathetic maturation *in vivo* (Figure S6E–S6F). Interestingly, using isolated samples from different regions of microfluidic chambers (Figure S6G), we found that expression levels of these genes were significantly higher in the neurons isolated from the proximal region (closer to NMVM) than the distal region (far from NMVM), implying that the higher probability of direct contact, the higher neuronal maturation occurs (Figure S6H–S6I). On the other hand, the co-cultured NMVM showed significant transcriptional changes of different cardiac marker genes (Figure S6J), indicating that the co-culturing with sympathetic neurons might affect the cellular phenotype of NMVM. However, the co-culture condition did not change the state of cardiomyocytes itself, including spontaneous beating rates, cell densities, and degrees of cell fusion status (Figure S6K–S6M). Overall, these data suggest that hPSC-derived sympathetic neurons undergo maturation when they are functionally and physically connected with ventricular myocytes.

Discussion

Previous reports demonstrated that hPSCs can be directed into multiple cell types, including neurons (Brennand et al., 2011; Dimos et al., 2008; Li et al., 2005; Maroof et al., 2010) and cardiomyocytes (Laflamme et al., 2007). However, modeling intercellular physiology with hPSCs remains a challenge owing to the absence of a proper model system. In the present study, we demonstrated the sequential development of human sympathetic neurons with four independent genetic reporter hPSC lines engineered by CRISPR/Cas9 technology (Cong et al., 2013; Mali et al., 2013), and the hPSC-derived sympathetic neuron’s physical and functional connectivity with cardiac muscle cells (ventricular myocytes). The direct differentiation and prospective isolation of sympathetic neurons from hPSCs described here is to sufficiently model their stepwise development and functional connection on cardiac syncytia. This approach offers unique opportunities for *in vitro* modeling human sympathetic neurons in the context of mechanistic insight on human neuronal development and interaction with their target tissues under physiological and pathophysiological conditions.

Like migrating sympathoadrenal neural crests in developing animal embryos (Morikawa et al., 2009; Saito et al., 2012; Schneider et al., 1999), activation of SHH and BMP signaling pathways appears crucial for our sympathetic neuronal specification with hPSC-based system (Figure 1G–1J and S1C–S1D), which allows us to recapitulate human sympathetic neuron specification *in vitro*. Our characterization of the *in vitro* molecular profile and functional properties shows that they are similar to those of their *in vivo* counterparts, including the expression of autonomic/sympathetic marker genes, catecholaminergic enzymes, capacity for NE-release, and electrophysiological profiles, such as phasic/tonic APs and medium AHP (Figure 1L, 2E–2H, 3B–3I, 5E–5F, S2D, S3A–S3I, and S3L–S3V).

Interestingly, small numbers of NMVM showed decreased beating rates after neuronal stimulation with nicotine (Figure 4D, *iii*) and a subset of PHOX2B::eGFP+ cells co-expressed cholinergic marker genes along with catecholaminergic markers (Figure S4O). Therefore, we speculate that our PHOX2B::eGFP+ cells exhibit functional cholinergic feature, potentially explaining the results of Figure 4D-*iii*. It will be intriguing to determine how hPSCs can sub-specify into other autonomic neuronal sub-lineages, including parasympathetic neurons and enteric neurons, with additional extrinsic morphogens and signaling cues, or different progenitors, such as peripheral glial cells (Dyachuk et al., 2014; Gershon, 2010).

Modeling diseases of the autonomic nervous system for personalized medicine has been challenging. Our PHOX2B::eGFP+ neuronal population provides a unique tool with which to dissect the molecular and cellular aspects of sympathetic specification under physiological conditions, as well as in the presence of congenital autonomic disorders. Our cell specification system can be readily applicable to disease-specific hiPSCs, which will allow us to generate and characterize sympathetic neurons from patients carrying genetic mutations that affect autonomic development and function (Axelrod et al., 2002; Chaudhuri, 2001; Kimura et al., 2012; Mudd and Kass, 2008; Rotthier et al., 2012; Vinik et al., 2003).

The ability of sympathetic neurons to control the behaviors of target tissues also provides an opportunity through which to understand neural modulation. As demonstrated in Figure 4B–4C and S4A–S4I, our hPSC-derived PHOX2B::eGFP+ sympathetic neurons can physically associate with cardiac tissues, and ultrastructural analysis shows that putative synaptic vesicles are located in the distal part of the neurons, resembling the early stage of neuromuscular synaptic formation. In addition, pharmacological stimulation (by nicotine treatment) or optogenetic stimulation (by optical control of channelrhodopsin) of our hPSC-derived PHOX2B::eGFP+ sympathetic neurons increased the beating rate of the connected cardiac syncytia (Figure 4D and 5G). However, hPSC-derived cardiomyocytes co-cultured with human sympathetic neurons did not show a detectable response to neuronal stimulation (with pharmacological stimulation, $n = 12$, data not shown). Potential explanation for this issue could be because: *i)* the co-culture condition may not be sufficient to make functional connections between hPSC-derived cardiomyocytes and human sympathetic neurons, *ii)* hPSC-derived cardiomyocytes may be still immature to make functional connection with sympathetic neurons, *iii)* hPSC-derived sympathetic neurons may be still immature to make functional connection with hPSC-derived cardiomyocytes. Further study to determine the suitable co-culture condition and aging/maturation of neurons and cardiomyocytes will be of great interest. Multiple target tissues are controlled by the sympathetic system, and it will be interesting to see whether our PHOX2B::eGFP+ sympathetic neurons, in conjunction with the autonomic circuitry of the central nervous system, can be connected to, and regulate, the other target organs and tissues, such as blood vessels, bone marrow, and brown adipocytes (Katayama et al., 2006; Perino et al., 2014; Takahashi et al., 2013). Thus it can be used to study the mechanisms of neuronal innervation and to model diseases resulted from pathologic sympathetic activation.

Another interesting finding in the co-culture of PHOX2B::eGFP+ sympathetic neurons and cardiac syncytia was that these functional connections confer maturation phenotypes on the

cultured neurons (Figure 6). This observation is in agreement with previous studies in animal models (Onteniente et al., 1992; Sheen et al., 1999), where functional connections of neurons with target organs can lead to neuronal maturation. Likewise, we noticed increased sensitivity to nicotine and elevated levels of both catecholaminergic enzyme expression and NE secretion (Figure 6). These maturation phenotypes elicited by functional connections between human sympathetic neurons and ventricular myocytes can provide insights into maturation of hPSC-derived neurons, which previously has been a challenge, limiting the modeling of neurodegenerative disorders and transplantation with 'age-matching' cells (Saha and Jaenisch, 2009). Because hESCs remain at the preimplantation stage, and the reprogramming of somatic cells into hiPSCs resets 'biological clocks', the hESC- and hiPSC-derived neurons can be mostly in embryonic and fetal stages. Therefore, functional interaction between the neurons and target tissues could be a 'natural' stimulating cue for the neuronal maturation process, as presented in our data (Figure 6). Complementary to the approach using over-expressing progerin, a truncated form of lamin A, which provides a model for understanding the epigenetic and genetic mechanisms underlying neural maturation (Miller et al., 2013), our findings will broaden understanding of human neuronal development as well as the general stem cell field in the context of modeling postnatal, even late onset, neural disorders.

In summary, our study provides a framework for the generation of distinct peripheral sympathetic neurons and an *in vitro* platform for 'sympathetic-cardiac neuromodulation in a dish', to study the neuronal regulation of cardiac behaviors implicated in many cardiac and autonomic diseases.

Experimental Procedures

Isolation of Neonatal Mouse Ventricular Myocytes (NMVM)

NMVM were isolated from 1-day-old C57BL/6 mice ventricles. In brief, the heart was quickly removed from the chest and rinsed one time with 70% EtOH and PBS. After removal of lung tissue, larger vessels, and atria under stereomicroscope, we chopped the ventricles and transfer small pieces of ventricles into 50 mL conical tube with digestion buffer (for enzymatic digestion, collagenase type II (0.4 mg/mL, Worthington) and pancreatin (0.2 mg/mL, Sigma-Aldrich) were added into the isolation solution (116 mM NaCl, 5.4 mM KCl, 5.5 mM glucose, 0.8 mM $MgSO_4$, 1 mM NaH_2PO_4, and 20 mM HEPES, adjusted to pH 7.4 with NaOH)). Then, put the tube in 37°C water bath for 30 min with shaking. Enzymes were inactivated after NMVM isolation by adding the mouse cardiomyocytes medium, which contains DMEM and Medium 199 in a 4:1 ratio supplemented with 10% FBS and 1% penicillin/streptomycin.

Details of Culture Condition

Please see the Table S1 for more details about culture conditions in every assay we presented. The table contains the information of each Figure number, hPSC-derived neurons or others (source, final cell type, number of days since the pluripotent stage, number of days after lentiviral transduction), myocytes (source, final cell type, number of days after isolation or differentiation), and co-culture (number of days after co-culture).

Pharmacological Control on Spontaneous Beating Rates of NMVM

Measurement of the spontaneous beating rate was performed as described previously (Devic et al., 2001) with slight modifications. In brief, 1–2 × 10^5 isolated NMVM (5 × 10^5 for optical mapping) were added onto hESC-derived sympathetic neurons (4–15 days after PHOX2B::eGFP+ sorting), sensory neurons, or mock with 1:1 mixed medium (mouse cardiomyocytes medium : neuron medium). 7–9 days after co-culture, the culture plates were placed in a temperature regulation apparatus positioned on the stage of an inverted microscope (Eclipse TE2000-E). Cells were equilibrated at 37°C for 10 min before monitoring the beating rate. A syncytium physically connected with neurites was selected for recording. For calculating beating rates of cells within the syncytium, a video was recorded for 1 min each before and 6 min after the stimulation of hESC-derived sympathetic neurons by 1 μM (−)-nicotine hemisulfate (Sigma-Aldrich). The data were analyzed using Prism.

Optogenetic Control on Spontaneous Beating Rates of NMVM

Optogenetic approaches were performed by using humanized channelrhodopsin-2 (hChR2)-infected hESC-derived sympathetic neurons. After packaging hChR2 lentivirus using pLenti-EF1a-hChR2(H134R)-EYFP-WPRE construct (Addgene plasmid #20942), hESC-derived sympathetic neurons (1–2 days after PHOX2B::eGFP+ sorting) were infected with hChR2 or eGFP lentivirus. The efficiency was checked by YFP or eGFP expression under fluorescence microscope. For eliminating residual virus particles on the well, infected wells were repetitively washed with culture medium and cultured them further with changing medium daily for at least 2 days. Then, 1–2 × 10^5 isolated neonatal mouse cardiomyocytes were added onto lentivirus-infected hESC-derived sympathetic neurons (total 4–15 days after PHOX2B::eGFP+ sorting) or mock, with 1:1 mixed medium (mouse cardiomyocytes medium : neuron medium). 7–8 days after co-culture, the culture plates were placed in a temperature regulation apparatus positioned on the stage of an inverted microscope (Eclipse TE2000-E). Cells were equilibrated at 37°C for 10 min before monitoring the beating rate. For calculating beating rates of cells within the syncytium, a video was repetitively recorded before and after illumination with continuous wide-field blue light (26 mW/mm^2 at 488 nm) for ~20 sec. Light intensity was measured on the focal plane with an optical power meter (LaserCheck, Coherent). The data were analyzed using Prism.

Statistical Analysis

Values are from at least three independent experiments with multiple replicates each, and reported as mean ± S.E.M. or mean + S.E.M. Differences between two samples were analyzed for significance using the unpaired Student's *t*-test in Sigma Plot 11. Differences between more than two groups were analyzed for significance using the ANOVA test in the Partek Genomics Suite.

Supplementary Material

Refer to Web version on PubMed Central for supplementary material.

Acknowledgments

We wish to acknowledge the services of Hao Zhang of the Johns Hopkins School of Public Health Flow Cytometry Core Facility for carrying out the cell sorting. We thank Jean-François Brunet (INSERM U1024, Paris F-75005, France) and Carmen Birchmeier (Max-Delbrück-Center for Molecular Medicine, Robert-Rössle-Strasse 10, 13125 Berlin, Germany) for generously sharing the PHOX2B and INSM1 antibody used in this study. We also thank Rejji Kuruvilla (Department of Biology, Johns Hopkins University, Baltimore, MD 21218, USA) for generously sharing the dissected SCG tissues, and Arun Venkatesan (Department of Biomedical Engineering, Johns Hopkins University School of Medicine, Baltimore, MD 21287, USA) for sharing the microfluidic chambers. Work in the Lee lab was supported by grants from Robertson Investigator Award from New York Stem Cell Foundation (G.L.) and Maryland Stem Cell Research Funding (MSCRF/TEDCO) (G.L.). The authors (G.L., Y.O.) acknowledge the joint participation by the Adrienne Helis Malvin Medical Research Foundation through its direct engagement in the continuous active conduct of medical research in conjunction with The Johns Hopkins Hospital and the Johns Hopkins University School of Medicine and the Foundation's Parkinson's Disease Program No. M-2014. C.K. supported by grants from NIH, MSCRF, TMTM. All microarray data used in this study have been deposited to NCBI's Gene Expression Omnibus (GEO; http://www.ncbi.nlm.nih.gov/geo) under accession number GEO: GSE80689.

References

Anderson DJ, Groves A, Lo L, Ma Q, Rao M, Shah NM, Sommer L. Cell lineage determination and the control of neuronal identity in the neural crest. Cold Spring Harb Symp Quant Biol. 1997; 62:493–504. [PubMed: 9598383]

Anderson RL, Jobling P, Gibbins IL. Development of electrophysiological and morphological diversity in autonomic neurons. J Neurophysiol. 2001; 86:1237–1251. [PubMed: 11535673]

Axelrod FB, Goldberg JD, Ye XY, Maayan C. Survival in familial dysautonomia: Impact of early intervention. J Pediatr. 2002; 141:518–523. [PubMed: 12378191]

Bharmal S, Slonimsky JD, Mead JN, Sampson CP, Tolkovsky AM, Yang B, Bargman R, Birren SJ. Target cells promote the development and functional maturation of neurons derived from a sympathetic precursor cell line. Dev Neurosci. 2001; 23:153–164. [PubMed: 11509838]

Bhatt S, Diaz R, Trainor PA. Signals and switches in mammalian neural crest cell differentiation. Cold Spring Harb Perspect Biol. 2013; 5:a008326. [PubMed: 23378583]

Brennand KJ, Simone A, Jou J, Gelboin-Burkhart C, Tran N, Sangar S, Li Y, Mu Y, Chen G, Yu D, et al. Modelling schizophrenia using human induced pluripotent stem cells. Nature. 2011; 473:221–225. [PubMed: 21490598]

Chambers SM, Fasano CA, Papapetrou EP, Tomishima M, Sadelain M, Studer L. Highly efficient neural conversion of human ES and iPS cells by dual inhibition of SMAD signaling. Nat Biotechnol. 2009; 27:275–280. [PubMed: 19252484]

Chambers SM, Qi Y, Mica Y, Lee G, Zhang XJ, Niu L, Bilsland J, Cao L, Stevens E, Whiting P, et al. Combined small-molecule inhibition accelerates developmental timing and converts human pluripotent stem cells into nociceptors. Nat Biotechnol. 2012; 30:715–720. [PubMed: 22750882]

Chaudhuri KR. Autonomic dysfunction in movement disorders. Curr Opin Neurol. 2001; 14:505–511. [PubMed: 11470968]

Cong L, Ran FA, Cox D, Lin S, Barretto R, Habib N, Hsu PD, Wu X, Jiang W, Marraffini LA, et al. Multiplex genome engineering using CRISPR/Cas systems. Science. 2013; 339:819–823. [PubMed: 23287718]

Cunningham M, Cho JH, Leung A, Savvidis G, Ahn S, Moon M, Lee PK, Han JJ, Azimi N, Kim KS, et al. hPSC-derived maturing GABAergic interneurons ameliorate seizures and abnormal behavior in epileptic mice. Cell Stem Cell. 2014; 15:559–573. [PubMed: 25517465]

Devay P, McGehee DS, Yu CR, Role LW. Target-specific control of nicotinic receptor expression at developing interneuronal synapses in chick. Nat Neurosci. 1999; 2:528–534. [PubMed: 10448217]

Devic E, Xiang Y, Gould D, Kobilka B. Beta-adrenergic receptor subtype-specific signaling in cardiac myocytes from beta(1) and beta(2) adrenoceptor knockout mice. Mol Pharmacol. 2001; 60:577–583. [PubMed: 11502890]

Dimos JT, Rodolfa KT, Niakan KK, Weisenthal LM, Mitsumoto H, Chung W, Croft GF, Saphier G, Leibel R, Goland R, et al. Induced pluripotent stem cells generated from patients with ALS can be differentiated into motor neurons. Science. 2008; 321:1218–1221. [PubMed: 18669821]

Dyachuk V, Furlan A, Shahidi MK, Giovenco M, Kaukua N, Konstantinidou C, Pachnis V, Memic F, Marklund U, Muller T, et al. Parasympathetic neurons originate from nerve-associated peripheral glial progenitors. Science. 2014; 345:82–87. [PubMed: 24925909]

Gershon MD. Developmental determinants of the independence and complexity of the enteric nervous system. Trends Neurosci. 2010; 33:446–456. [PubMed: 20633936]

Hirsch MR, Tiveron MC, Guillemot F, Brunet JF, Goridis C. Control of noradrenergic differentiation and Phox2a expression by MASH1 in the central and peripheral nervous system. Development. 1998; 125:599–608. [PubMed: 9435281]

Huber K, Bruhl B, Guillemot F, Olson EN, Ernsberger U, Unsicker K. Development of chromaffin cells depends on MASH1 function. Development. 2002; 129:4729–4738. [PubMed: 12361965]

Jobling P, Gibbins IL. Electrophysiological and morphological diversity of mouse sympathetic neurons. J Neurophysiol. 1999; 82:2747–2764. [PubMed: 10561442]

Joseph NM, Morrison SJ. Toward an understanding of the physiological function of mammalian stem cells. Dev Cell. 2005; 9:173–183. [PubMed: 16054025]

Katayama Y, Battista M, Kao WM, Hidalgo A, Peired AJ, Thomas SA, Frenette PS. Signals from the sympathetic nervous system regulate hematopoietic stem cell egress from bone marrow. Cell. 2006; 124:407–421. [PubMed: 16439213]

Kimura K, Ieda M, Fukuda K. Development, maturation, and transdifferentiation of cardiac sympathetic nerves. Circ Res. 2012; 110:325–336. [PubMed: 22267838]

Laflamme MA, Chen KY, Naumova AV, Muskheli V, Fugate JA, Dupras SK, Reinecke H, Xu C, Hassanipour M, Police S, et al. Cardiomyocytes derived from human embryonic stem cells in pro-survival factors enhance function of infarcted rat hearts. Nat Biotechnol. 2007; 25:1015–1024. [PubMed: 17721512]

Lee G, Kim H, Elkabetz Y, Al Shamy G, Panagiotakos G, Barberi T, Tabar V, Studer L. Isolation and directed differentiation of neural crest stem cells derived from human embryonic stem cells. Nat Biotechnol. 2007; 25:1468–1475. [PubMed: 18037878]

Li XJ, Du ZW, Zarnowska ED, Pankratz M, Hansen LO, Pearce RA, Zhang SC. Specification of motoneurons from human embryonic stem cells. Nat Biotechnol. 2005; 23:215–221. [PubMed: 15685164]

Mali P, Yang L, Esvelt KM, Aach J, Guell M, DiCarlo JE, Norville JE, Church GM. RNA-guided human genome engineering via Cas9. Science. 2013; 339:823–826. [PubMed: 23287722]

Maroof AM, Brown K, Shi SH, Studer L, Anderson SA. Prospective isolation of cortical interneuron precursors from mouse embryonic stem cells. J Neurosci. 2010; 30:4667–4675. [PubMed: 20357117]

Mica Y, Lee G, Chambers SM, Tomishima MJ, Studer L. Modeling neural crest induction, melanocyte specification, and disease-related pigmentation defects in hESCs and patient-specific iPSCs. Cell Rep. 2013; 3:1140–1152. [PubMed: 23583175]

Miller JD, Ganat YM, Kishinevsky S, Bowman RL, Liu B, Tu EY, Mandal PK, Vera E, Shim JW, Kriks S, et al. Human iPSC-based modeling of late-onset disease via progerin-induced aging. Cell Stem Cell. 2013; 13:691–705. [PubMed: 24315443]

Morikawa Y, Maska E, Brody H, Cserjesi P. Sonic hedgehog signaling is required for sympathetic nervous system development. Neuroreport. 2009; 20:684–688. [PubMed: 19349918]

Mudd JO, Kass DA. Tackling heart failure in the twenty-first century. Nature. 2008; 451:919–928. [PubMed: 18288181]

Onteniente B, Nothias F, Geffard M, Peschanski M. Maturation and fine structure of thalamic reticular neurons transplanted into the adult rat CNS. Dev Neurosci. 1992; 14:130–143. [PubMed: 1396173]

Pattyn A, Goridis C, Brunet JF. Specification of the central noradrenergic phenotype by the homeobox gene Phox2b. Mol Cell Neurosci. 2000; 15:235–243. [PubMed: 10736201]

Perino A, Beretta M, Kilic A, Ghigo A, Carnevale D, Repetto IE, Braccini L, Longo D, Liebig-Gonglach M, Zaglia T, et al. Combined inhibition of PI3Kbeta and PI3Kgamma reduces fat mass

by enhancing alpha-MSH-dependent sympathetic drive. Sci Signal. 2014; 7:ra110. [PubMed: 25406378]

Perrier AL, Tabar V, Barberi T, Rubio ME, Bruses J, Topf N, Harrison NL, Studer L. Derivation of midbrain dopamine neurons from human embryonic stem cells. Proc Natl Acad Sci U S A. 2004; 101:12543–12548. [PubMed: 15310843]

Rotthier A, Baets J, Timmerman V, Janssens K. Mechanisms of disease in hereditary sensory and autonomic neuropathies. Nat Rev Neurol. 2012; 8:73–85. [PubMed: 22270030]

Saha K, Jaenisch R. Technical challenges in using human induced pluripotent stem cells to model disease. Cell Stem Cell. 2009; 5:584–595. [PubMed: 19951687]

Saito D, Takase Y, Murai H, Takahashi Y. The dorsal aorta initiates a molecular cascade that instructs sympatho-adrenal specification. Science. 2012; 336:1578–1581. [PubMed: 22723422]

Schneider C, Wicht H, Enderich J, Wegner M, Rohrer H. Bone morphogenetic proteins are required in vivo for the generation of sympathetic neurons. Neuron. 1999; 24:861–870. [PubMed: 10624949]

Schrenk-Siemens K, Wende H, Prato V, Song K, Rostock C, Loewer A, Utikal J, Lewin GR, Lechner SG, Siemens J. PIEZO2 is required for mechanotransduction in human stem cell-derived touch receptors. Nat Neurosci. 2015; 18:10–16. [PubMed: 25469543]

Sheen VL, Arnold MW, Wang Y, Macklis JD. Neural precursor differentiation following transplantation into neocortex is dependent on intrinsic developmental state and receptor competence. Exp Neurol. 1999; 158:47–62. [PubMed: 10448417]

Steinbeck JA, Jaiswal MK, Calder EL, Kishinevsky S, Weishaupt A, Toyka KV, Goldstein PA, Studer L. Functional Connectivity under Optogenetic Control Allows Modeling of Human Neuromuscular Disease. Cell Stem Cell. 2016; 18:134–143. [PubMed: 26549107]

Takahashi Y, Sipp D, Enomoto H. Tissue interactions in neural crest cell development and disease. Science. 2013; 341:860–863. [PubMed: 23970693]

Vinik AI, Maser RE, Mitchell BD, Freeman R. Diabetic autonomic neuropathy. Diabetes Care. 2003; 26:1553–1579. [PubMed: 12716821]

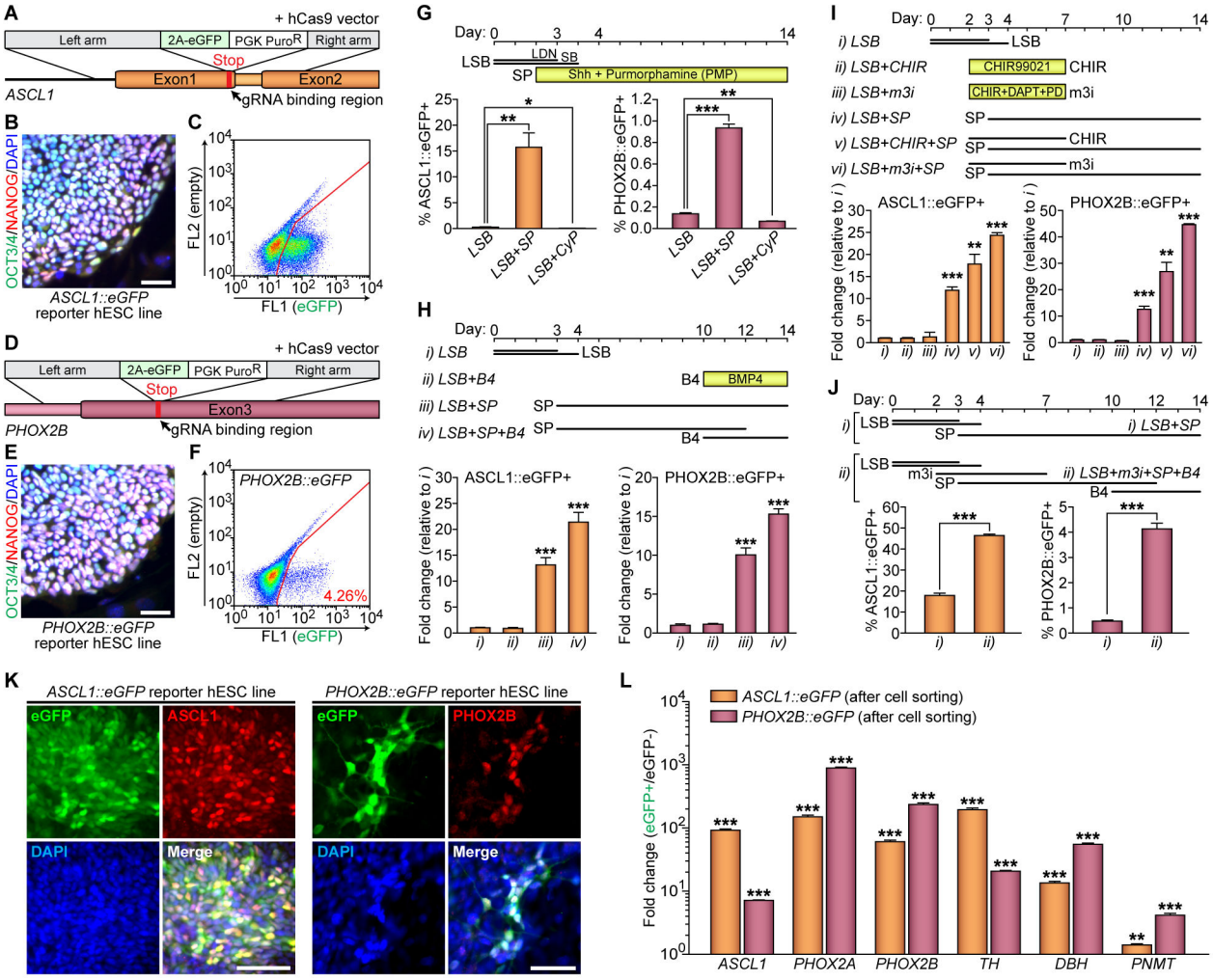

Figure 1. Activation of WNT Followed by SHH Signaling Leads Both ASCL1 and PHOX2B Inductions in hPSC-Derived Autonomic Specification

(A and D) Schematics for *ASCL1* and *PHOX2B* gene targeting using homologous recombination enhanced by CRISPR/Cas9 system. (B and E) Immunofluorescence analyses were performed using OCT3/4 (green) and NANOG (red) antibodies. Representative images of OCT3/4+/NANOG+ colonies from the undifferentiated *ASCL1::eGFP* (B) and *PHOX2B::eGFP* (E) reporter lines. (C and F) Representative FACS plots of differentiated reporter hESC lines for either (C) *ASCL1* or (F) *PHOX2B*. (G–J) Top, schematics for differentiation; bottom, after addition of (G) the recombinant sonic hedgehog C25II (Shh) protein and SHH agonist (purmorphamine, PMP) or SHH antagonist (cyclopamine, CyP) to the LSB protocol, (H) BMP4 (B4) to the LSB-SP protocol, (I) CHIR99021 (CHIR) and 'modified-3i' (m3i; CHIR, DAPT, and PD173074) to the LSB-SP protocol, or (J) m3i and B4 to the LSB protocol, the percentages of ASCL1::eGFP− and PHOX2B::eGFP-expressing cells was measured by using FACS analysis (* $P < 0.05$; ** $P < 0.01$; *** $P < 0.001$; unpaired Student's *t*-test; $n = 3$). LSB, LDN193189 and SB431542. SP, Shh plus PMP. (K) Immunofluorescence analyses were performed at day 10 following LSB (day 0–3/4) – m3i (day 2–7) – SP (day 3–10) treatment, using GFP (green) and either ASCL1 (red) or

PHOX2B (red) antibodies. (L) qRT-PCR data showing enrichments of each transcript after cell sorting (** $P < 0.01$; *** $P < 0.001$; compared to eGFP− population; unpaired Student's *t*-test; $n = 3$). All error bars represent mean + S.E.M. Scale bars, 50 μm. See also Figure S1.

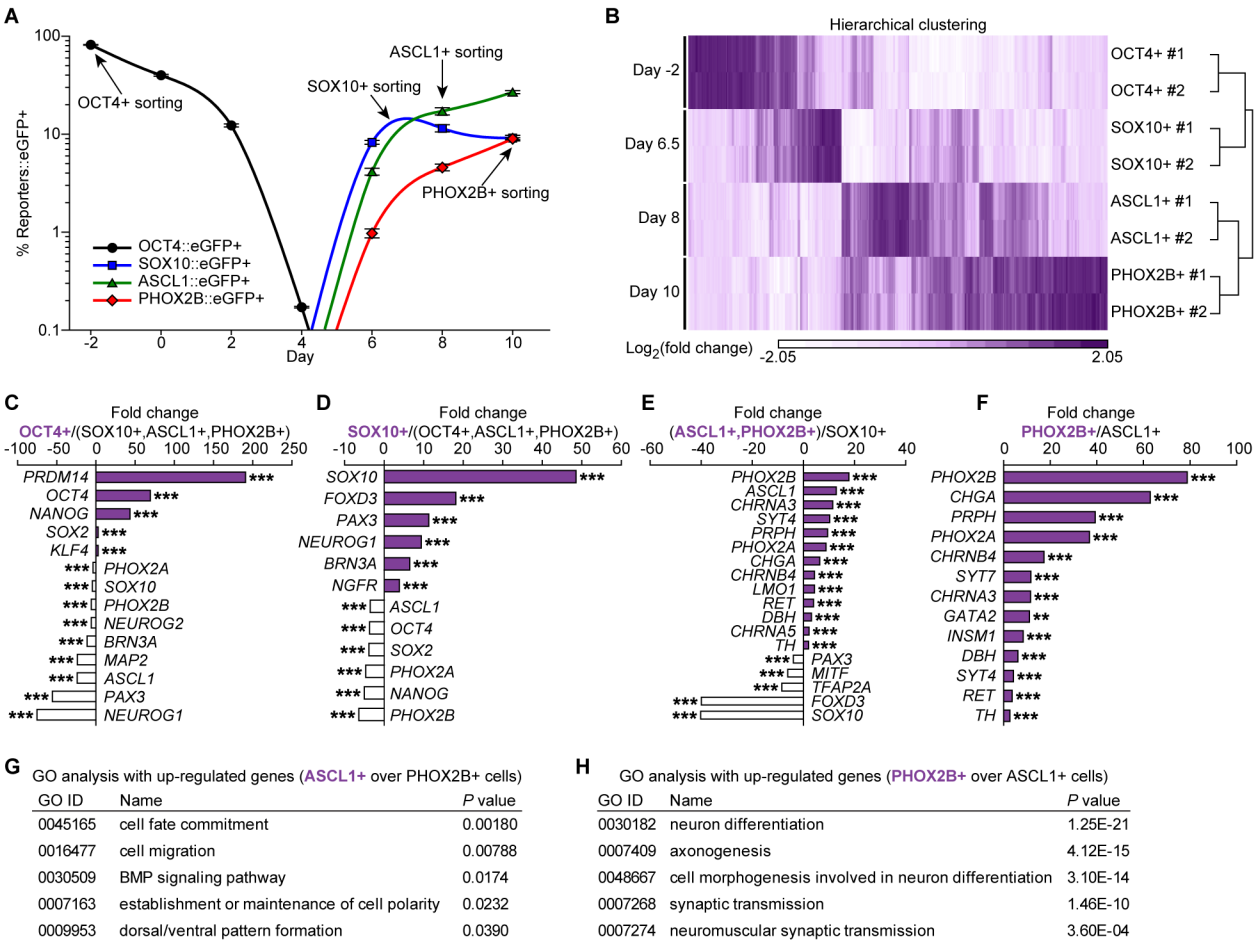

G GO analysis with up-regulated genes (**ASCL1+** over PHOX2B+ cells)

GO ID	Name	*P* value
0045165	cell fate commitment	0.00180
0016477	cell migration	0.00788
0030509	BMP signaling pathway	0.0174
0007163	establishment or maintenance of cell polarity	0.0232
0009953	dorsal/ventral pattern formation	0.0390

H GO analysis with up-regulated genes (**PHOX2B+** over ASCL1+ cells)

GO ID	Name	*P* value
0030182	neuron differentiation	1.25E-21
0007409	axonogenesis	4.12E-15
0048667	cell morphogenesis involved in neuron differentiation	3.10E-14
0007268	synaptic transmission	1.46E-10
0007274	neuromuscular synaptic transmission	3.60E-04

Figure 2. Genetic Reporter hPSC Lines for Four Different Genes Reveal Distinct Stages of Sympathetic Neuronal Differentiation

(A–H) Changes of each reporter gene expression after differentiation using different lines and protocols: for *OCT4::eGFP* and *SOX10::eGFP* lines: LSB (day 0–3/4) – CHIR (day 2–10); for *ASCL1::eGFP* line: LSB (day 0–3/4) – CHIR (day 2–7) – SP (day 3–10); for *PHOX2B::eGFP* line: LSB (day 0–3/4) – m3i (day 2–7) – SP (day 3–10). The eGFP positive samples were collected by cell sorting at the specific time points as indicated. LSB, LDN193189 and SB431542; m3i, CHIR (CHIR99021), DAPT, and PD173074; SP, Shh plus PMP (purmorphamine). (B) Clustered heat map of global gene expression after microarray analyses ($n = 2$). (C–F) List of the increased (purple) and decreased (white) genes comparing two groups, as assessed by microarray analysis (** $P < 0.01$; *** $P < 0.001$; ANOVA test using Partek Genomics Suite (Partek Inc.); $n = 3$ for OCT4+, SOX10+, or ASCL1+ cells; $n = 2$ for PHOX2B+ cells). (G–H) Gene ontology (GO) analysis with upregulated gene list (G, ASCL1+ cells over PHOX2B+ cells; H, PHOX2B+ cells over ASCL1+ cells). All error bars represent mean ± S.E.M. See also Figure S2.

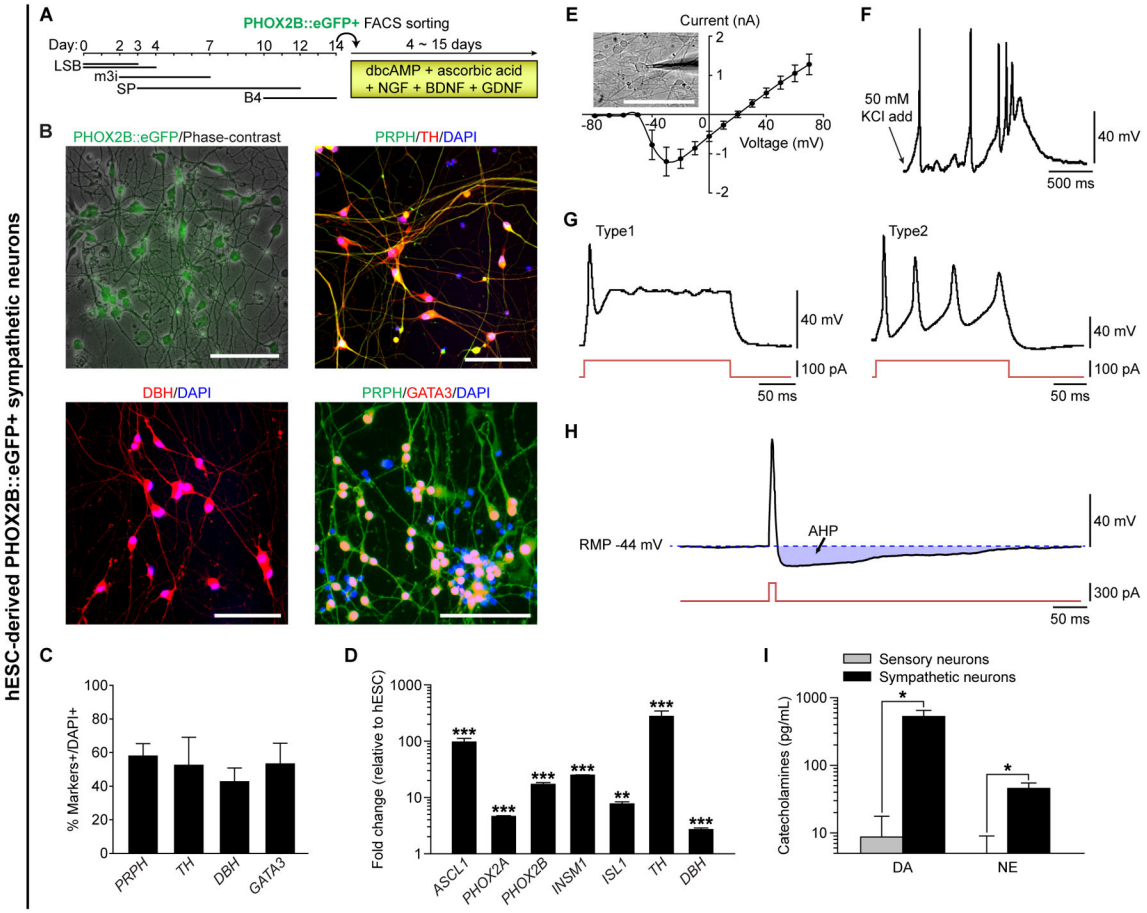

Figure 3. Characterization of FACS-Purified PHOX2B::eGFP+ Sympathetic Neurons from hPSCs

(A) Schematic for differentiation of PHOX2B::eGFP positive cells. LSB, LDN193189 and SB431542; m3i, CHIR99021, DAPT, and PD173074; SP, Shh plus PMP (purmorphamine). B4, BMP4. (B) FACS-purified PHOX2B::eGFP-expressing putative sympathetic neuronal precursors gave rise to peripherin (PRPH, pseudo-green), TH (red), DBH (red), GATA3 (red)-expressing sympathetic neurons. (C) Quantification of PRPH, TH, DBH, and GATA3 positive cells ($n = 3$). (D) qRT-PCR data showing significant increases of each transcript after sympathetic neuronal differentiation (**$P < 0.01$; ***$P < 0.001$; compared to each transcript level of undifferentiated hESCs; unpaired Student's t-test; $n = 3$). (E–H) Electrophysiological characterization of PHOX2B::eGFP-expressing sympathetic neurons, including (E) I–V curve ($n = 7$), representative action potentials upon either (F) administration of 50 mM KCl, or (G) injecting 100 pA current. In (E), 10 of 10 neurons express a considerable amount of sodium channels and potassium channel to conduct both inward and outward current. In (F), 3 of 4 neurons responded to 50 mM KCl. In (G), 4 of 9 neurons fired a single of action potential (Type 1) and 5 of 9 neurons fired a train of action potentials (Type 2); 8 of 9 neurons responded to currents of 100 pA or greater, and 1 (Type 1) of 9 neurons responded to currents of 300 pA or greater. (H) An action potential (top) evoked during a brief depolarizing current step (bottom), with an afterhyperpolarization (AHP); 3 of 4 neurons had medium AHP (lasts 221–428 ms); RMP, resting membrane

potential. (I) Release of catecholamines after 50 mM KCl administration were analyzed by using commercial ELISA kit (*$P < 0.05$; unpaired Student's *t*-test; $n = 3$). DA, dopamine. NE, norepinephrine. All error bars represent mean ± S.E.M. or mean + S.E.M. Scale bars, 100 μm. See also Figure S3.

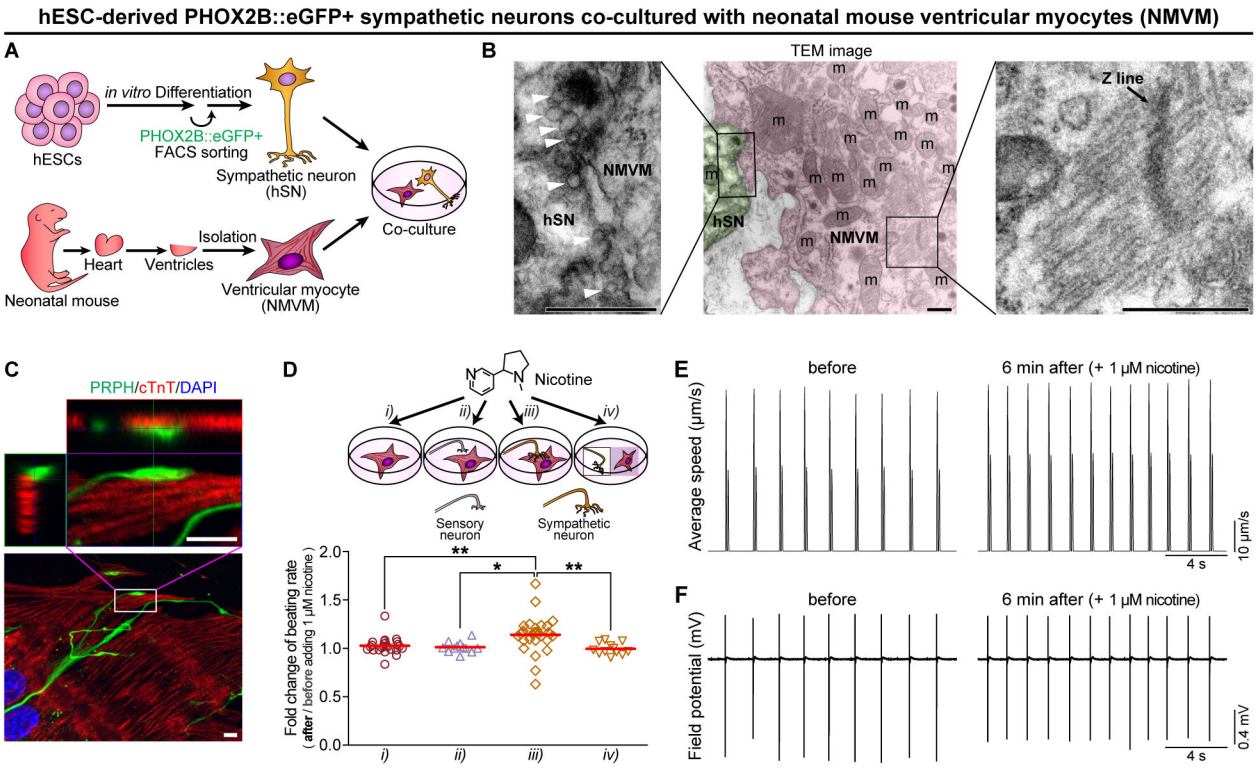

Figure 4. hPSC-Derived Sympathetic Neurons Can Pharmacologically Control Spontaneous Beating of Neonatal Mouse Ventricular Myocytes

(A) Schematic representation of the *in vitro* co-culture system, with FACS-purified human ESC-derived PHOX2B::eGFP+ sympathetic neurons (hSNs) and neonatal mouse ventricular myocytes (NMVM), used to test sympathetic-cardiac connections. (B) Transmission electron microscopy (TEM) image of the junctional region between hSN and NMVM following co-culture. Green-colored region indicates the nerve terminal of a hSN, and pink-colored region indicates the NMVM. White arrowheads indicate putative synaptic vesicles. (C) Immunofluorescence analysis was performed using PRPH (pseudo-green, hSNs) and cTnT (red, NMVM) antibodies. Bottom, maximum intensity projection of confocal microscopy z-stacks. Top, ortho-images of boxed region in the bottom image (*see* Movie S1 for 3-D reconstructed image). (D) Top, schematic diagrams for the control of beating rate of NMVM; bottom, increased beating rates were observed upon the administration of 1 μM nicotine (*see* Experimental Procedures; $*P < 0.05$; $**P < 0.01$; unpaired Student's *t*-test; $n =$ 25 for *i*, 12 for *ii*, 31 for *iii*, 12 for *iv*). Red lines indicate each mean value. (E–F) High speed video image acquisitions and multi-electrode array (MEA) recordings were synchronized (*see* Supplemental Experimental Procedures for more details). (E) Using motion vector analysis, increased beating rates were observed 6 min after administration of 1 μM nicotine. First peaks of each beating indicate contractions, and second peaks indicate relaxations. (F) Using MEA recordings, increased beating rates were detected 6 min after treatment of 1 μM nicotine. Scale bars in (B) TEM images, 0.5 μm; in (C) confocal images, 5 μm. See also Figure S4 and Movie S1–S3.

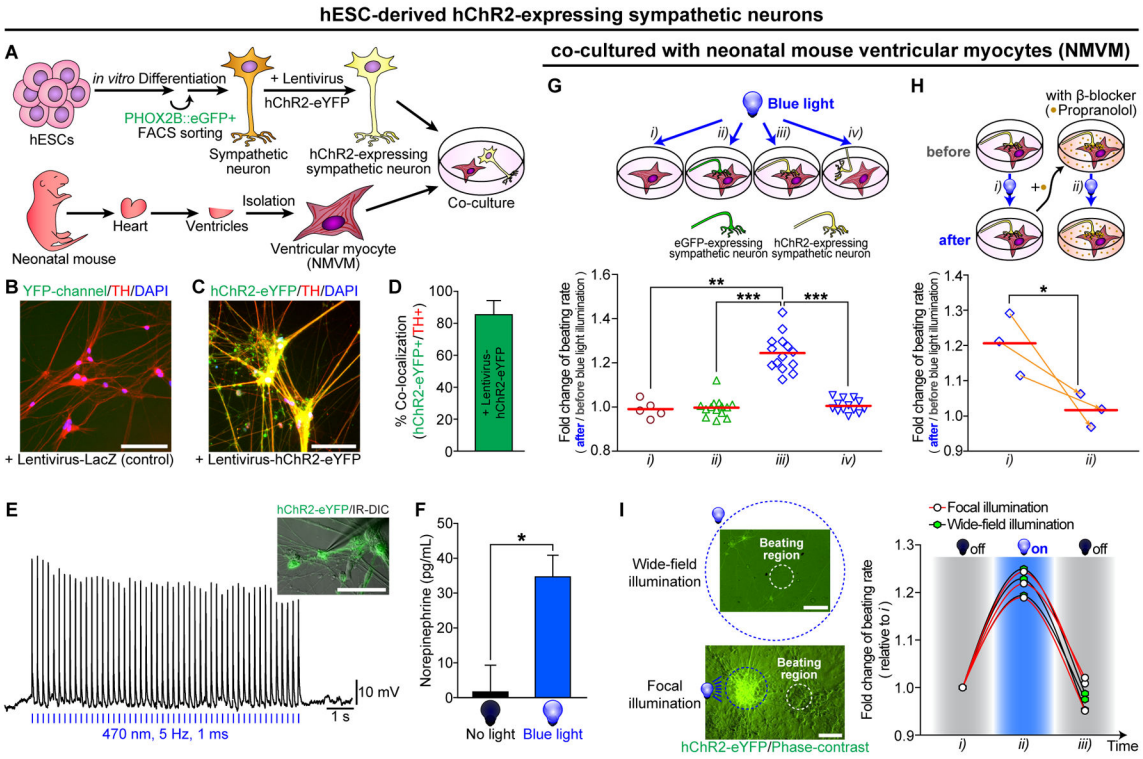

Figure 5. Optogenetic Control on hPSC-derived Sympathetic Neurons Lead to Changes of Spontaneous Beating of Neonatal Mouse Ventricular Myocytes

(A) Schematic representation of the *in vitro* co-culture system, with FACS-purified human ESC-derived hChR2-expressing PHOX2B::eGFP+ sympathetic neurons and neonatal mouse ventricular myocytes (NMVM), for testing sympathetic-cardiac connections. hESC-derived sympathetic neurons were infected with (C–I) hChR2 or (B) LacZ lentivirus. (B–C) Immunofluorescence analyses were performed using TH (red) antibody. (D) Quantification of the proportion of co-localized cells ($n = 6$). (E) Cultured sympathetic neurons-expressing hChR2-eYFP were targeted in IR-DIC for whole-cell patch clamp recordings. Responses of a neuron to trains of wide-field blue light pulses at a constant frequency (20 mW at 470 nm, 5 Hz, 1 ms) were represented. (F) The amounts of norepinephrine release after 15 min illumination with continuous wide-field blue light (26 mW/mm^2 at 488 nm) or no light, were analyzed by using commercial ELISA kit (*$P < 0.05$; unpaired Student's *t*-test; $n = 3$). (G–H) Top, schematic diagrams for the control of beating rate of NMVM; bottom, (G) increased beating rates were observed upon the photoactivation of hChR2-expressing sympathetic neurons with continuous wide-field blue light (*see* Experimental Procedures; 26 mW/mm^2 at 488 nm; **$P < 0.01$; ***$P < 0.001$; unpaired Student's *t*-test; $n = 5$ for *i*, $n = 14$ for *ii*, $n = 14$ for *iii*, $n = 13$ for *iv*). (H) Before and after treatment of β-blocker (1 μM propranolol) for 5 min, neuronal-photostimulation-induced beating rate change on NMVM was measured (*$P < 0.05$; unpaired Student's *t*-test; $n = 3$). Orange arrows connect the data, before and after treatment of 1 μM propranolol, obtained from the same NMVM syncytium. Red lines indicate each mean value. (I) Photoactivation of hChR2-expressing sympathetic neurons co-cultured with NMVM using continuous wide-field blue light or continuous focal blue light. Different from conventional wide-field illumination, the field diaphragm in the epi-

illumination pathway of the microscope was fully closed in order to achieve focal illumination (area, 0.08 mm^2). Light intensity was 26 mW/mm^2 at 488 nm. (I, left panel) Example images representing focal and wide-field illumination. Blue dotted circle indicates an illuminated region with blue light. White dotted circle indicates a beating region of NMVM. (I, right panel) With focal ($n = 3$) or wide-field ($n = 3$) illumination, spontaneous beating rates were measured in the order of three sections (~20 sec each): *i)* 'no illumination just before photostimulation', *ii)* 'blue light illumination for photostimulation', and *iii)* 'no illumination just after photostimulation'. All error bars represent mean + S.E.M. Scale bars, 100 μm. See also Figure S5 and Movie S4.

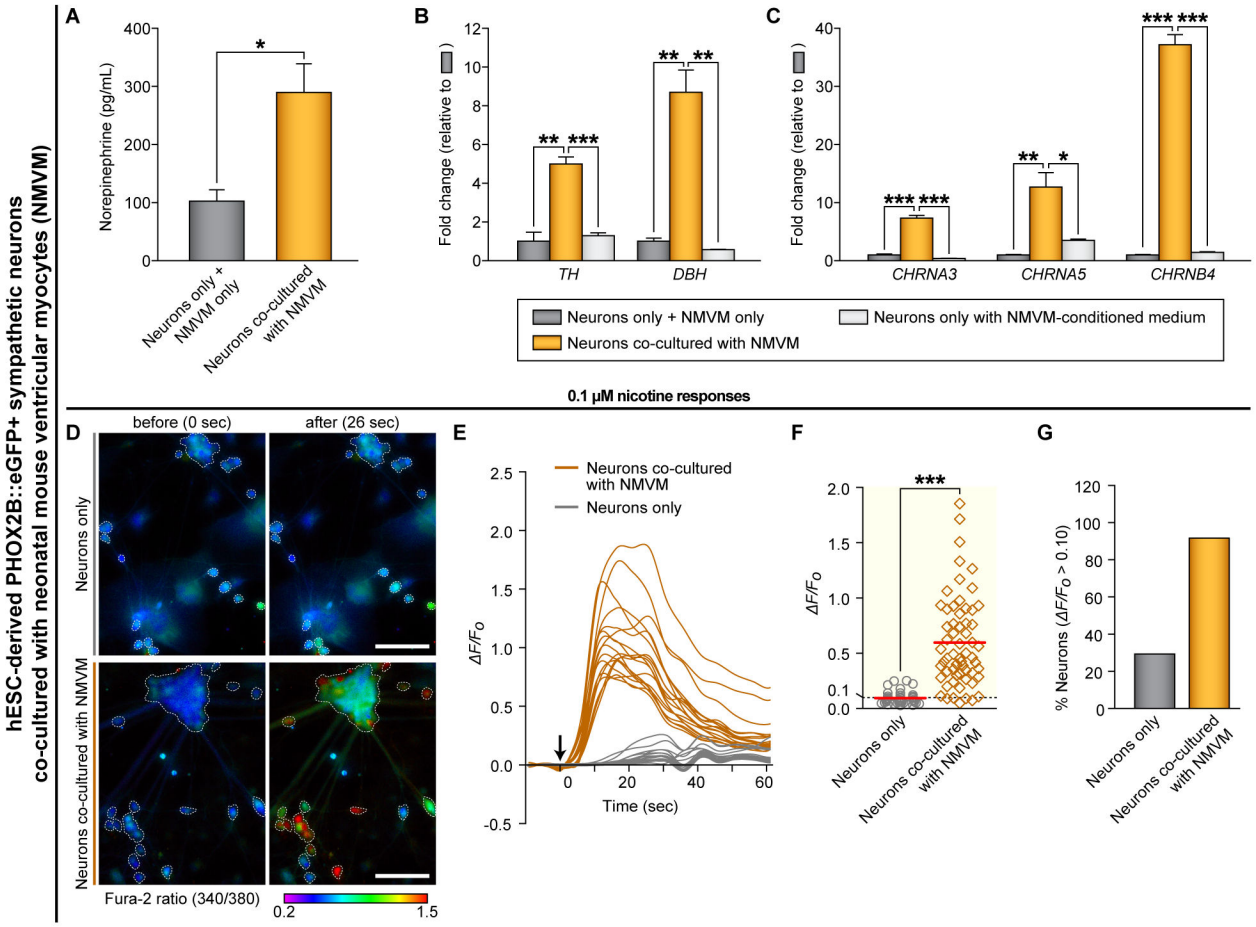

Figure 6. Physical Interaction Between hPSC-Derived Sympathetic Neurons and Ventricular Myocytes Leads to Neuronal Maturation Phenotypes

(A) The amounts of norepinephrine release after 50 mM KCl administration were analyzed by using commercial ELISA kit (*$P < 0.05$; unpaired Student's t-test; $n = 3$). Neurons, hESC-derived PHOX2B::eGFP+ sympathetic neurons. NMVM, neonatal mouse ventricular myocytes. (B–C) We used the 'neurons only with NMVM-conditioned medium' control (one day conditioned medium of NMVM was collected and fed to 'neuron only' sample daily for 7 days). The RNA from 'neurons only' samples and 'NMVM only' samples were mixed together and used as a 'neurons only + NMVM only' control. qRT-PCR analyses were performed by using indicated human-specific primers (*$P < 0.05$; **$P < 0.01$; ***$P < 0.001$; unpaired Student's t-test; $n = 3$). (D–G) The changes in intracellular calcium concentrations $[Ca^{2+}]_i$ induced by 0.1 μM nicotine were measured by ratiometric Fura-2 imaging. Calcium responses were calculated as the ratio of Fura-2 light emission on excitation at 340 and 380 nm (340/380) or the normalized ratio ($\Delta F/F_0$; $\Delta F = (F - F_0)$, F = the 340/380 at a given time point, F_0 = the mean basal, unstimulated 340/380 of each cell). White boundaries in (D) indicate the cell bodies of neurons which satisfy the criterion for selecting neurons as described in Supplemental Experimental Procedures. (E) Example traces of $\Delta F/F_0$ intensity from the neurons co-cultured with (dark orange lines) or without (gray lines) NMVM exposed to 0.1 μM nicotine. Each trace is a response from a unique cell

(n = 18). (F) $\Delta F/F_0$ intensity plot showing the response of individual cells to 0.1 μM nicotine (***P < 0.001; unpaired Student's t-test; neurons only, n = 41; neurons with cardiomyocytes, n = 60). Red lines indicate each mean value. (G) The percent of total responder neurons ($\Delta F/F_0$ > threshold) in each sample. All error bars represent mean + S.E.M. See also Figure S6 and Movie S5.